JCTC Journal of Chemical Theory and Computation

Article

pubs.acs.org/JCTC

^{1}H Chemical Shifts in Paramagnetic Co(II) Pyrazolylborate Complexes: A First-Principles Study

Syed Awais Rouf, Jiří Mareš, and Juha Vaara*

NMR Research Group, University of Oulu, P.O. Box 3000, FIN-90014 Oulu, Finland

Supporting Information

ABSTRACT: We apply the theory of the nuclear magnetic resonance (NMR) chemical shift for paramagnetic systems to demanding cobalt(II) complexes. Paramagnetic NMR (pNMR) chemical shift results by density-functional theory (DFT) can be very far from the experimental values. Therefore, it is of interest to investigate the applicability of electron-correlated *ab initio* computational methods to achieve useful accuracy. Here, we use *ab initio* wave function based electronic structure methods to calculate the pNMR chemical shift within the theoretical framework established recently. We applied the *N*-electron valence-state perturbation theory (NEVPT2) on three Co(II) systems, where the active space of the underlying complete active space self-consistent field (CASSCF) wave function consists of seven electrons in the five metal 3*d* orbitals. These complexes have the $S = 3/2$ electronic ground state consisting of two doublets separated by zero-field splitting (ZFS). To calculate the hyperfine coupling tensor $\boldsymbol{A}$, DFT was used, while the $\boldsymbol{g}$- and ZFS-tensors were calculated using the *ab initio* CASSCF and NEVPT2 methods. These results were combined to obtain the total chemical shifts. The shifts obtained from these calculations are in generally good agreement with the experimental results, in some cases suggesting a reassignment of the signals. The accuracy of this mixed *ab initio*/DFT approach is very promising for further applications to demanding pNMR problems involving transition metals.

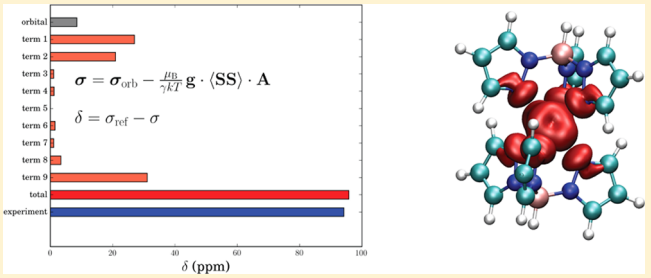

1. INTRODUCTION

Nuclear magnetic resonance (NMR) is an efficient technique to investigate the structural and dynamical properties of materials of interest in physics, chemistry, biology, and medicine.[1] The NMR technique is used for both electronically closed- and open-shell systems.[2−5] The NMR parameters (nuclear shielding and spin−spin coupling) for diamagnetic, closed-shell systems are routinely calculated by using the Ramsey theory.[6−8] This theory is extensively used in the computational determination of the NMR parameters by applying electronic structure methods,[9−11] including relativistic contributions in systems containing heavy elements.[12] However, the methods for accurate calculation of the NMR parameters of paramagnetic (open-shell) systems are still not very well-developed.[13]

Important milestones in the conceptual development of the chemical shift theory of paramagnetic NMR (pNMR) were laid by McConnell and co-workers, who introduced the contact and dipolar hyperfine shifts[14] as well as the pseudocontact shift.[15] Kurland and McGarvey[16] worked out the principles of taking into account the zero-field splitting (ZFS) interaction, unquenched orbital moments, and thermally populated excited states. Moon and Patchkovskii[17] presented an elegant framework for doublet systems (with one unpaired electron) that was easily implemented into an electronic structure code.[18] A practical model for first-principles calculations of pNMR chemical shifts, incorporating also ZFS effects, was developed by Pennanen and Vaara in 2008[19] by extending the findings of ref 17 to higher-than doublet multiplicities. This method includes the contributions of the $2S+1$ states (S is the quantum number of the effective electron spin) of the electronic ground-state manifold and assumes it to be described by the ZFS Hamiltonian of the form $H_{\mathrm{ZFS}} = \boldsymbol{S}\cdot\boldsymbol{D}\cdot\boldsymbol{S}$, where $\boldsymbol{D}$ is the ZFS-tensor and $\boldsymbol{S}$ is the effective spin operator. An underlying approximation of the method is that the spin−orbit coupling is relatively weak and that the higher-order ZFS and Zeeman interactions can be neglected.[20] Soncini and Van den Heuvel[21] pointed out that the shielding expression of ref 19 does not reproduce the correct low-temperature limiting behavior of the pNMR shifts. The error of ref 19 lies in the omission of the magnetic couplings between the states belonging to the ground-state manifold. This is easily fixed, and the present paper uses the corrected formalism.

Later advances in the computations of pNMR shifts have been made in the improved incorporation of relativistic effects, such as the inclusion of scalar relativity in all-electron calculations by Autschbach et al.[22,23] and the fully relativistic, 4-component formulation of the doublet case by Komorovsky et al.[24] Van den Heuvel and Soncini[20,25] presented a more general formulation of the pNMR shielding theory in which no limitation to the weak spin−orbit coupling had to be resorted to. The shielding tensor in this approach is presented in terms

Received: November 29, 2014

DOI: 10.1021/acs.jctc.5b00193
J. Chem. Theory Comput. XXXX, XXX, XXX−XXX

of the generalized g- (parametrizing the Zeeman interaction) and hyperfine coupling (HFC) tensors, and in cases where these are available beyond the ground-state ZFS manifold, the method allows the incorporation of also such electronically excited states that do not arise from the ground-state manifold. Formulation in terms of the generalized property tensors that are not routinely calculated represents a limitation for the large-scale application of the method, however. The presently employed method [based on eq 1, see below] is a more elementary but computationally straightforward extension of the Pennanen-Vaara model for the ground-state ZFS manifold, which has been made to include the magnetic couplings between the states and is compatible with the findings of ref 21. In particular, the present method incorporates the contributions of the lowest electronically excited states. Finally, Martin and Autschbach[26] investigated analytically the temperature dependence for systems of different spin multiplicities, using the formula of Soncini and Van den Heuvel.[21]

So far most of the modern pNMR shielding computations have been performed at the density-functional theory (DFT) level, as reviewed in ref 13. It has been found[27,28] that DFT has problems in accurate ZFS calculations, necessary in systems with the electron spin quantum number $S > 1/2$ and, at times, also for the g-tensor. pNMR chemical shift computations need to be made more accurate, and one way of doing this is to apply high-level calculations based on *ab initio* wave function theory (WFT).[29] It is important to know the general accuracy attainable from the currently available shift computations, because extensions are necessary and planned to include both cases with strong spin−orbit coupling effects and the influence of low-lying electronically excited states, other than those belonging to the zero-field split ground-state manifold.[20] Both of these situations occur, *e.g.*, in paramagnetic lanthanide and actinide complexes.

As examples of demanding transition-metal systems, the proton (^{1}H) NMR shifts for three different pyrazolylborate complexes of the 3d Co(II) ion were reported experimentally by Długopolska et al.[30] The computations also carried out in that paper, based on DFT and an outdated shielding formalism, were not able to convincingly relate to the experimental results. We show in the present paper that to obtain a good agreement with the experimental data of ref 30, both modern shielding theory[19,21] and high-level computations of the relevant ZFS and Zeeman interactions are needed. In this article, we calculate the ^{1}H NMR shifts for the three different pyrazolylborate complexes of Co(II) that were published in the paper by Długopolska et al.[30] We use the complete active space self-consistent field (CASSCF)[31] and N-electron valence state perturbation theory[32−35] (NEVPT2) methods for these parameters.[36] The HFC ($\boldsymbol{A}$) tensors involved in the pNMR shielding expression were calculated by DFT, both using the generalized gradient approximation (GGA, with the PBE functional[37]) and hybrid DFT (PBE0[38]). It should be noted that multiconfigurational WFT methods have already earlier been applied in the context of pNMR shielding by Van den Heuvel and Soncini[20] in their general formulation and by Rinkevicius et al.[39] within the elementary nonrelativistic doublet-state theory.

The results of these calculations for the three different Co(II) complexes are mostly in very good agreement with experimental shifts, provided that a few reassignments of the measured chemical shifts to the different groups of protons are made. We suggest such reassignments based on the computations of the present kind, which are promising for further applications to transition-metal systems.

2. THEORY AND COMPUTATIONAL METHODS

2.1. Theory. The theory of the pNMR chemical shift presented in ref 19 gave an approximate expression for the part of the nuclear shielding tensor that is independent of the magnetic field. This expression can be made exact within the limitation to the ground-state ZFS manifold and relatively weak spin−orbit coupling, by introducing the magnetic couplings, arising from the Zeeman and HFC interactions, between the states belonging to different degenerate manifolds:

$$\boldsymbol{\sigma} = \boldsymbol{\sigma}_{orb} - \frac{\mu_B}{\gamma kT}\, \boldsymbol{g}\cdot\langle \boldsymbol{SS}\rangle \cdot \boldsymbol{A} \tag{1}$$

$$\langle \boldsymbol{SS}\rangle = \frac{\sum_{nm} Q_{mn}\langle n|\boldsymbol{S}|m\rangle\langle m|\boldsymbol{S}|n\rangle}{\sum_n \exp(-E_n/kT)} \tag{2}$$

$$Q_{mn} = \begin{cases} \exp(-E_n/kT) & E_n = E_m \\ -\dfrac{kT}{E_m - E_n}[\exp(-E_m/kT) & E_n \neq E_m \\ \quad - \exp(-E_n/kT)] & \end{cases} \tag{3}$$

where γ, μ_B, k, and T are the gyromagnetic ratio of the nucleus, Bohr magneton, Boltzmann constant, and absolute temperature, respectively. $\langle \boldsymbol{SS}\rangle$ is a dyadic with the components $\langle S_\sigma S_\tau\rangle$ evaluated in the manifold of electronic states $|n\rangle$ (with energies E_n), consisting of the ground-state zero-field split spin multiplet. In eq 1, the first term is the orbital shielding, which is approximately independent of the temperature.[6,7,39] The second, hyperfine shielding term consists of the generalized product of the g-tensor, $\langle \boldsymbol{SS}\rangle$, and the HFC tensor $\boldsymbol{A}$. This formula is compatible with the results of Soncini and Van den Heuvel.[21]

The isotropic shielding constant and the chemical shift are obtained from the calculated shielding tensor by using

$$\sigma = \frac{(\sigma_{xx} + \sigma_{yy} + \sigma_{zz})}{3} \tag{4}$$

$$\delta = \sigma_{ref} - \sigma \tag{5}$$

respectively. Here σ, σ_{ref}, and δ are the isotropic shielding constant of the nucleus in question in the investigated molecule, the shielding constant of the same isotope in a diamagnetic reference compound (in our case tetramethylsilane, TMS), and the chemical shift, respectively. In using eq 1, the HFC tensor can be decomposed as

$$\boldsymbol{A} = A_{con}\mathbf{1} + \boldsymbol{A}_{dip} + A_{pc}\mathbf{1} + \boldsymbol{A}_{dip,2} + \boldsymbol{A}_{as} \tag{6}$$

where $\mathbf{1}$ is a 3 × 3 unit matrix, and A_{con} as well as $\boldsymbol{A}_{dip}$ are the nonrelativistic isotropic contact coupling and anisotropic dipolar coupling tensors, respectively. A_{pc} is the isotropic pseudocontact coupling, $\boldsymbol{A}_{dip,2}$ is the anisotropic and symmetric "second dipolar term", and $\boldsymbol{A}_{as}$ is the antisymmetric term. These three contributions are due to the perturbational relativistic spin−orbit (SO) corrections to HFC,[40] the use of which is justified for the light ligand nuclei in 3d complexes. The g-tensor can, in turn, be decomposed as

$$\boldsymbol{g} = g_e\mathbf{1} + \Delta g_{iso}\mathbf{1} + \Delta\tilde{\boldsymbol{g}} \tag{7}$$

DOI: 10.1021/acs.jctc.5b00193
J. Chem. Theory Comput. XXXX, XXX, XXX−XXX

where g_e is the free-electron g-factor, while Δg_{iso} and $\Delta\tilde{\boldsymbol{g}}$ are the isotropic and anisotropic parts of the $\boldsymbol{g}$-shift tensor (deviation from the isotropic g_e-value).

Experimentally, the pNMR shifts are often analyzed as[2]

$$\delta_{exp} = \delta_{orb} + \delta_{con}^{exp} + \delta_{pc}^{exp} \tag{8}$$

where terms arising from several distinct physical mechanisms are bundled together. However, by electronic structure calculations of the various terms implied by eq 1 [with the decompositions of $\boldsymbol{A}$ and $\boldsymbol{g}$ as in eqs 6 and 7, respectively], it is possible to reveal the full structure. Theoretically, the contributions to the isotropic chemical shift up to the order $O(\alpha^4)$ in the fine structure constant α are given as

$$\delta_{theory} = \delta_{orb} + \delta_{con} + \delta_{con,2} + \delta_{con,3} + \delta_{dip} + \delta_{dip,2} + \delta_{dip,3} + \delta_{c,aniso} + \delta_{pc} \tag{9}$$

The detailed breakdown of the various contributions to the total shift resulting from the terms of $\boldsymbol{g}$ and $\boldsymbol{A}$ is given in Table 1. To establish a correspondence with the experimental chemical shift, we can group the theoretical terms as

$$\delta_{con}^{exp} = \delta_{con} + \delta_{con,2} + \delta_{con,3} \tag{10}$$

$$\delta_{pc}^{exp} = \delta_{dip} + \delta_{dip,2} + \delta_{dip,3} + \delta_{c,aniso} + \delta_{pc} \tag{11}$$

Table 1. Classification of the Nuclear Shielding Terms in Paramagnetic Molecules of Higher than Doublet Spin Multiplicity

term in $\sigma_{e\tau}$	term identifier	symbol	order[a]	rank[b]
σ_{orb}	orb	δ_{orb}	$O(\alpha^2)$	0, 2, 1
$g_e A_{con}\langle S_e S_\tau\rangle$	first	δ_{con}	$O(\alpha^2)$	0, 2
$g_e\sum_b A_{b\tau}^{dip}\langle S_e S_b\rangle$	second	δ_{dip}	$O(\alpha^2)$	0, 2, 1
$g_e A_{PC}\langle S_e S_\tau\rangle$	third	$\delta_{con,2}$	$O(\alpha^4)$	0, 2
$g_e\sum_b A_{b\tau}^{dip,2}\langle S_e S_b\rangle$	fourth	$\delta_{dip,2}$	$O(\alpha^4)$	0, 2, 1
$g_e\sum_b A_{b\tau}^{as}\langle S_e S_b\rangle$	fifth	δ_{as}	$O(\alpha^4)$	2, 1
$\Delta g_{iso} A_{con}\langle S_e S_\tau\rangle$	sixth	$\delta_{con,3}$	$O(\alpha^4)$	0, 2
$\Delta g_{iso}\sum_b A_{b\tau}^{dip}\langle S_e S_b\rangle$	seventh	$\delta_{dip,3}$	$O(\alpha^4)$	0, 2, 1
$A_{con}\sum_a \Delta\tilde{g}_{ea}\langle S_a S_\tau\rangle$	eighth	$\delta_{c,aniso}$	$O(\alpha^4)$	0, 2, 1
$\sum_{ab}\Delta\tilde{g}_{ea}A_{b\tau}^{dip}\langle S_a S_b\rangle$	ninth	δ_{pc}	$O(\alpha^4)$	0, 2, 1

[a]Order in the fine structure constant α in which the terms appear in. [b]Contributions with tensorial ranks 0, 2, and 1 correspond to the isotropic shielding constant, anisotropic and symmetric, as well as anisotropic and antisymmetric terms, respectively.

The experimental chemical shift term δ_{con}^{exp} of eq 10 corresponds to the sum of three theoretical terms that appear indistinguishably in eq 9. Similarly, the term δ_{pc}^{exp} bundles five terms of different origins [given in eq 11] to the experimental pseudocontact shift. However, it is noteworthy that of the contributions to δ_{pc}^{exp}, only three terms (δ_{dip}, $\delta_{dip,3}$, δ_{pc}) contain the spin-dipolar hyperfine operator, whereas the other two terms ($\delta_{dip,2}$ and $\delta_{c,aniso}$) do not.[19,41] This is important from the point-of-view of using the pseudocontact shifts for the structural determination of paramagnetic molecules, based on the functional form of the spin-dipole operator. The structural information extracted from δ_{pc} may at intermediate distances from the metal center be contaminated by the nondipolar $\delta_{dip,2}$ and $\delta_{c,aniso}$ mechanisms.[41] Also note that the δ_{as} term does not contribute to the isotropic shift at all.

2.2. Computational Methods. Electronic structure calculations were carried out for both the experimental X-ray and computationally optimized geometries for the three Co(II) complexes depicted in Figure 1. The experimental structures were obtained from ref 30. The coordination of the cobalt ion is slightly distorted octahedral in these systems (Figure 1). The geometry optimization was carried out on the TURBOMOLE software[42] using the B3LYP[43−45] functional with the def2-TZVP[46,47] basis set for the light atoms. For the Co center, the Stuttgart-type energy-consistent small-core (10 electrons in the core), scalar-relativistic effective core potential ECP10MDF,[48] and the appropriate 8*s*7*p*6*d*2*f*1*g*/6*s*5*p*3*d*2*f*1*g* (in the primitive/contracted notation) valence basis set[49] were used. The optimized structures are given in the Supporting Information. The terms needed for computing the pNMR chemical shifts were calculated by two different software packages, i.e., GAUSSIAN 09 (G09)[50] and ORCA.[36] The computations of σ_{orb} were carried out with G09 and those of $\boldsymbol{g}$, $\boldsymbol{D}$, and $\boldsymbol{A}$ with ORCA.[51−53] The computations for σ_{orb} and $\boldsymbol{A}$ were performed at the DFT level with the PBE and PBE0 functionals, while the computations of $\boldsymbol{g}$ and $\boldsymbol{D}$ were done with *ab initio* WFT at the CASSCF and NEVPT2 levels. While DFT can be assumed to perform reasonably well for σ_{orb}, using DFT for the $\boldsymbol{A}$-tensors represents a more critical approximation, dictated by the lack of software efficient enough for pursuing HFC calculations at a good enough, correlated WFT level for the present systems. We also present a comparison to calculations in which DFT (PBE) was used also for $\boldsymbol{g}$ and $\boldsymbol{D}$, in the case of system 1. The notation used throughout the article for these calculations is CASSCF/DFT(PBE) or NEVPT2/DFT(PBE) denoting combined methods where either CASSCF or NEVPT2 was used for $\boldsymbol{g}$ and $\boldsymbol{D}$, whereas PBE was used for $\boldsymbol{A}$. Similarly, in CASSCF/DFT(PBE0) or NEVPT2/DFT(PBE0) calculations PBE0 was employed for $\boldsymbol{A}$. The active space in our state-average CASSCF calculations, which also underlie the NEVPT2 calculations, consisted of the seven metal *d*-electrons in the five Co(3*d*) orbitals. All 10 quartet and 40 doublet states allowed by the CAS(7,5) calculation were included.

The HFC tensors needed for the chemical shifts were calculated with DFT using different exchange-correlation functionals. In these calculations, the GGA PBE and the hybrid PBE0 functional, the latter with 25% exact exchange admixture, were used with the all-electron def2-SVP, def2-TZVP, and def2-QZVPP[46,47] basis sets applied for all the atoms. For systems 1 and 2, we also employed the PBE50 functional, where the exact exchange admixture has been raised to 50%. The basis sets used for the $\boldsymbol{g}$- and $\boldsymbol{D}$-tensor calculations were of the locally dense basis-set (LDBS) type,[54−56] i.e., for the metal ion and the atoms directly bonded to it, we used a better basis sets such as TZVP, while for the other atoms we used the SVP basis. The purpose of these LDBS calculations is to reduce the computational cost; the spin density distribution that gives rise to $\boldsymbol{g}$ and $\boldsymbol{D}$ is localized in the immediate neighborhood of the metal ion. Therefore, the LDBS (denoted as TZVP*, etc.) calculations perform equally well as, and are less expensive than, the calculations with the fully balanced (FB, e.g., TZVP) basis set. However, the HFC calculations were performed with the same FB basis set for all the atoms because of the high sensitivity of this property to the quality of the basis set, particularly at those centers for which the HFC is needed. The corresponding designations for the basis sets are SVP/SVP, TZVP*/SVP,

DOI: 10.1021/acs.jctc.5b00193
J. Chem. Theory Comput. XXXX, XXX, XXX−XXX

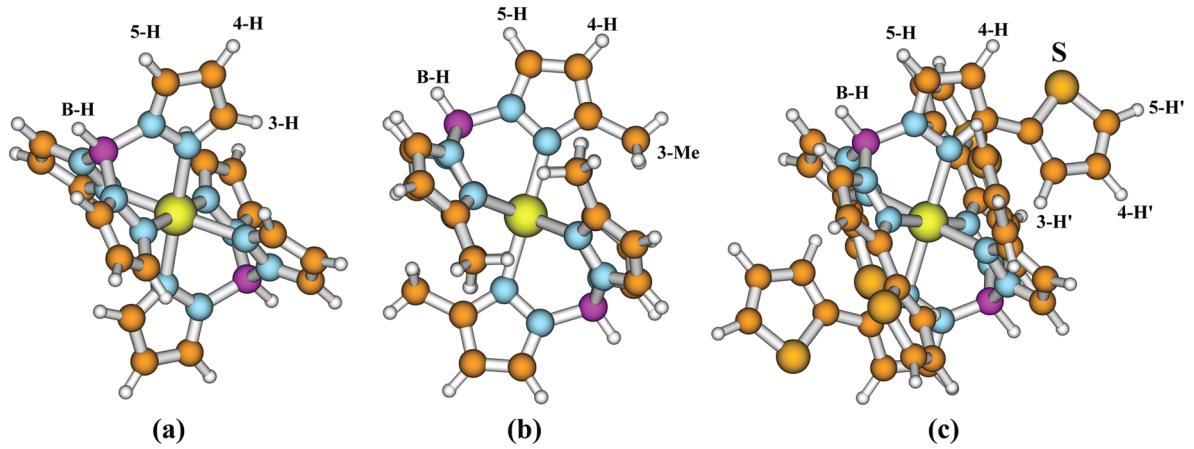

Figure 1. High-spin Co(II) pyrazolylborate complexes investigated in this paper: (a) system 1, (b) system 2, and (c) system 3. The distinct groups of hydrogens, for which the chemical shifts were calculated, are indicated.

SVP/TZVP, TZVP*/TZVP, and QZVPP*/QZVPP, where the first basis set specified is used for ***g*** and ***D***, while the second set is used for ***A***. A comparison of the results obtained for system 1 with LDBS and FB basis set is given in Table 2.

Table 2. Chemical Shifts Calculated by Using the Locally Dense TZVP* Basis Set (LDBS) and Fully Balanced (FB) TZVP Basis Set for System 1 at the Optimized Geometry

	LDBS/TZVP*[a]		FB/TZVP[b]	
nucleus	CASSCF	NEVPT2	CASSCF	NEVPT2
3-H	94.6	95.5	93.4	94.3
4-H	38.4	38.3	36.9	36.9
5-H	−90.1	−92.2	−91.9	−93.9
B-H	126.5	128.5	125.1	127.1

[a]DFT(PBE0) was used for calculation of ***A*** using the full TZVP basis, while CASSCF and NEVPT2 were used to calculate ***g*** and ***D*** with LDBS (TZVP*). [b]DFT(PBE0) was used for calculation of ***A***, while CASSCF and NEVPT2 were used to calculate ***g*** and ***D*** with FB (TZVP used throughout).

The calculated shieldings were averaged within the experimentally equivalent group of nuclei. The chemical shifts are reported with respect to TMS, for which the calculated ^{1}H shielding constants (with only the orbital contribution) are reported in Table S4 in the Supporting Information. The geometry of TMS was optimized using the TURBOMOLE program. The ^{1}H nuclear shielding for this closed-shell molecule was calculated with G09 using DFT with the same exchange-correlation functionals and basis sets as used for the present Co(II) complexes. All the shielding and shift calculations were done using the temperature of 298 K.

3. RESULTS AND DISCUSSION

3.1. DFT Performance for Zero-Field Splitting and *g*-Tensor. The DFT performance was evaluated by calculating ***g*** and ***D*** for system 1 at the experimental geometry and comparing the resulting chemical shifts with *ab initio* calculations as well as experiment. The DFT calculations were carried out with the PBE functional and two different basis sets (SVP and TZVP). Using DFT for ***g*** and ***D*** causes large deviations in the chemical shifts from the experimental data, as evident from Table 3. The DFT-based chemical shift pattern does not correspond to the experimental one, even if a reassignment of the experimental signals were performed. Therefore, to increase the accuracy, we applied higher levels of theory for the critical ***g***- and ***D***-tensors, in this case the CASSCF and NEVPT2 methods. The NEVPT2 results for the ***g***- and ***D***-tensors provide a much improved correspondence with the experimental chemical shift values as compared to DFT calculations. The reasons of the apparent failure of the all-DFT approach to the chemical shifts are evident from the comparison of the DFT and NEVPT2 ***g*** and ***D***, placed in Table S5 in the Supporting Information. For DFT(PBE) with the TZVP basis, the isotropic *g*-value is 2.076 and the *D*-parameter of ZFS equals −7.009 cm^{-1}, whereas at the CASSCF and NEVPT2 levels (with the TZVP* basis), much larger values, particularly *D* at around 112 cm^{-1}, are found. These values show a very large difference between the ZFS magnitudes, which implies differing chemical shifts, too. DFT under-

Table 3. Comparison of Chemical Shifts Obtained from DFT (PBE) and *ab Initio*/DFT(PBE) Calculations for System 1 at the Experimental Geometry

	DFT(PBE)[a]		CASSCF/DFT(PBE)[b]		NEVPT2/DFT(PBE)[c]		
nucleus	SVP	TZVP	SVP	TZVP	SVP	TZVP	exp[30]
3-H	39.9	52.7	96.6	110.4	96.9	110.8	−111.0
4-H	51.1	59.9	41.4	50.8	41.6	51.2	42.0
5-H	45.0	35.0	−74.2	−82.9	−74.1	−82.5	94.2
B-H	−4.0	−4.5	133.4	130.5	133.5	130.4	122.0

[a]DFT(PBE) used for all the σ_{orb}-, ***A***-, ***g***-, and ***D***-tensors. [b]DFT(PBE) used for calculation of σ_{orb} and ***A*** with the indicated basis sets, while CASSCF was used to calculate ***g*** and ***D*** with the SVP and TZVP* basis sets. [c]DFT(PBE) used for calculation of σ_{orb} and ***A*** with the indicated basis sets, while NEVPT2 was used to calculate ***g*** and ***D*** with the SVP and TZVP* basis sets.

DOI: 10.1021/acs.jctc.5b00193
J. Chem. Theory Comput. XXXX, XXX, XXX−XXX

Table 4. Effects of the Basis Set, Selection of the Wave Function (in the Calculations of the *g*- and *D*-Tensors), the DFT Functional (in the Calculation of the *A*-Tensor), and the Structure (Experimental x-Ray or Computationally Optimized) on the ^{1}H Chemical Shifts (in ppm) of System 1

level	other parameters	3-H	4-H	5-H	B-H
Effect of Basis[a] for *g*, *D*/*A*					
SVP/SVP	NEVPT2/PBE0	87.2	31.4	−86.6	131.4
TZVP*/SVP	NEVPT2/PBE0	86.5	31.7	−84.6	129.6
SVP/TZVP	NEVPT2/PBE0	96.1	38.0	−94.2	130.3
TZVP*/TZVP	NEVPT2/PBE0	95.5	38.3	−92.2	128.5
SVP/QZVPP	NEVPT2/PBE0	96.8	40.0	−92.7	128.8
TZVP*/QZVPP	NEVPT2/PBE0	96.1	40.3	−90.8	127.0
QZVPP*/QZVPP[b]	NEVPT2/PBE0	95.8	40.0	−90.9	126.6
Effect of Wave Function for *g* and *D*					
CASSCF/PBE0	TZVP*/TZVP	94.6	38.4	−90.1	126.5
NEVPT2/PBE0	TZVP*/TZVP	95.5	38.3	−92.2	128.5
Effect of DFT Functional[c] for *A*					
NEVPT2/PBE	TZVP*/TZVP	112.5	60.2	−70.3	121.6
NEVPT2/PBE0	TZVP*/TZVP	95.5	38.3	−92.2	128.5
NEVPT2/PBE50	TZVP*/TZVP	88.4	24.7	−103.2	133.8
Effect of Structure[d] on *A*					
NEVPT2/PBE0(EXP)	TZVP*/TZVP	93.5	32.5	−100.0	136.9
NEVPT2/PBE0(OPT)	TZVP*/TZVP	95.5	38.3	−92.2	128.5
best[e]		95.8	40.0	−90.9	126.6
exp.[f]		94.2	42.0	−111.0	122.0

[a]CASSCF and NEVPT2 were used at the optimized geometry to calculate *g* and *D* with SVP, TZVP*, and QZVPP* (the latter two were LDBS) basis sets, and the *A* results were obtained with DFT(PBE0) using fully balanced basis sets. [b]σ_{orb} was calculated with the TZVP basis sets, while *g* and *D* were calculated with the QZVPP* basis sets and *A* with the QZVPP basis sets at the NEVPT2/PBE0 level. [c]DFT (PBE, PBE0, and PBE50 functionals) was used at the optimized geometry for calculations of *A*. [d]Calculation at the experimental geometry denoted by EXP and one at the optimized geometry denoted by OPT. [e]Best calculated value at the NEVPT2 level for *g* and *D* with the QZVPP* basis set and *A* with fully balanced QZVPP at the PBE0 level, all at the optimized structure. [f]Reference 30. Experimentally observed values. A significant difference is found with the original experimental assignment for 3-H and 5-H. Therefore, we made a signal reassignment between these two nuclei, with the result that the shifts are rendered into a very good agreement with the experiment.

Table 5. Effects of the Basis Set, Selection of the Wave Function (in the Calculations of the *g*- and *D*-Tensors), the DFT Functional (in the Calculation of the *A*-Tensor), and the Structure (Experimental or Computationally Optimized) on the ^{1}H Chemical Shifts of System 2

level	other parameters	3-H	4-H	5-H	B-H
Effect of Basis[a] for *g*, *D*/*A*					
SVP/SVP	NEVPT2/PBE0	−86.8	31.5	80.0	133.1
TZVP*/SVP	NEVPT2/PBE0	−85.5	31.6	79.2	131.0
SVP/TZVP	NEVPT2/PBE0	−86.8	38.8	86.7	131.0
TZVP*/TZVP	NEVPT2/PBE0	−85.5	38.9	85.9	128.9
Effect of Wave Function for *g* and *D*					
CASSCF/PBE0	TZVP*/TZVP	−82.3	39.3	83.6	123.6
NEVPT2/PBE0	TZVP*/TZVP	−85.5	38.9	85.9	128.9
Effect of DFT Functional[b] for *A*					
NEVPT2/PBE	TZVP*/TZVP	−76.5	61.2	98.2	122.0
NEVPT2/PBE0	TZVP*/TZVP	−85.5	38.9	85.9	128.9
NEVPT2/PBE50	TZVP*/TZVP	−90.9	25.7	81.2	133.6
Effect of Structure[c] on *A*					
NEVPT2/PBE0(EXP)	TZVP*/TZVP	−96.6	34.7	88.5	143.2
NEVPT2/PBE0(OPT)	TZVP*/TZVP	−85.5	38.9	79.2	128.9
best[d]		−85.5	38.9	85.9	128.9
exp[e]		−100.1	49.5	2.2	90.0

[a]CASSCF and NEVPT2 were used with the optimized geometry to calculate *g* and *D* with SVP and TZVP* (the latter with LDBS) basis sets, and the *A* results were obtained with DFT(PBE0) using fully balanced basis sets. [b]DFT (PBE, PBE0, and PBE50 functionals) was used at the optimized geometry for calculations of *A*. [c]Calculation at the experimental geometry denoted by EXP and the one at the optimized geometry denoted by OPT. [d]Best calculated value calculated at the NEVPT2 level for *g* and *D* with the TZVP* basis set and *A* with the fully balanced TZVP basis at the PBE0 level, all at the optimized structure. [e]Reference 30. Experimentally observed values.

estimates the *g*- and *D*-values. The static correlation contained in the modest CASSCF wave function used presently is able to significantly correct the magnitude of the *D*-parameter. In contrast, for this system, the dynamical correlation treatment applied at the NEVPT2 level only brings in a relatively small change on top of the CASSCF data. It is suggested based already on these calculations that there is a misassignment of the experimental shifts between the equally abundant nuclei 3-H and 5-H, possibly due to different numbering conventions used in this paper and in ref 30. In the following sections we will present more refined calculations with the *ab initio* methodology applied to *g* and *D*.

3.2. System 1. Table 4 reports a summary of the calculated results for system 1. The full data are given in Table S6 in the Supporting Information. It is important to use a good basis to get high-accuracy results. The effect of basis set can be seen by comparing NEVPT2/PBE0 results obtained with the SVP and TZVP basis sets, as given in Table 4. It shows that the difference of chemical shifts obtained with the basis-set patterns SVP/SVP and TZVP*/SVP (the first indicated basis used for *g* and *D*, the second for *A*) for nuclei 3-H, 4-H, 5-H, and B-H are 0.7, 0.3, 2.0, and 1.8 ppm, respectively, with similar changes of values obtained between basis sets SVP/TZVP and TZVP*/TZVP. However, up to 9 ppm change in the chemical shift of 3-H is obtained when the HFC is calculated with the TZVP or QZVPP basis sets as compared to SVP. This shows that there is only a small effect of the basis set for *g* and *D* but a much larger effect of the basis set for *A*. However, the difference of only 2 ppm or less is seen when the HFC is calculated with QZVPP as compared to the TZVP basis set, in Table 4.

The change of chemical shift with the choice of the wave function used for the *g*- and *D*-tensors is also given in Table 4.

DOI: 10.1021/acs.jctc.5b00193
J. Chem. Theory Comput. XXXX, XXX, XXX−XXX

Table 6. Effects of the Basis Set, Selection of the Wave Function (in the Calculations of the *g*- and *D*-Tensors), the DFT Functional (in the Calculation of the *A*-Tensor), and the Structure (Experimental or Computationally Optimized) on the ^{1}H Chemical Shifts of System 3

level	other parameters	3-H′	4-H′	5-H′	4-H	5-H	B-H
Effect of Basis[a] for ***g***, ***D***/***A***							
SVP/SVP	NEVPT2/PBE0	0.2	−0.3	−21.5	83.6	37.8	119.7
TZVP*/SVP	NEVPT2/PBE0	0.5	0.0	−20.6	82.0	38.2	115.3
SVP/TZVP	NEVPT2/PBE0	−1.9	−0.3	−24.4	74.5	47.4	108.3
TZVP*/TZVP	NEVPT2/PBE0	−1.6	0.0	−23.4	72.8	47.7	103.9
Effect of Wave Function for ***g*** and ***D***							
CASSCF/PBE0	TZVP*/TZVP	−0.8	0.6	−22.3	69.5	48.2	95.8
NEVPT2/PBE0	TZVP*/TZVP	−1.6	0.0	−23.4	72.8	47.7	103.9
Effect of DFT Functional[b] for ***A***							
NEVPT2/PBE	TZVP*/TZVP	−3.4	0.7	−26.6	77.4	72.4	97.2
NEVPT2/PBE0	TZVP*/TZVP	−1.6	0.0	−23.4	72.8	47.7	103.9
Effect of Structure[c] on ***A***							
CASSCF/PBE0(EXP)	TZVP*/TZVP	−4.6	−5.7	−44.1	66.4	38.5	105.6
CASSCF/PBE0(OPT)	TZVP*/TZVP	−0.8	0.6	−22.3	69.5	48.2	95.8
best[d]		−1.6	0.0	−23.4	72.8	47.7	103.9
exp[e]		−0.7	0.2	−25.1	65.4	47.5	83.3

[a]NEVPT2 was used at the optimized geometry to calculate ***g*** and ***D*** with SVP and TZVP* (the latter with LDBS) basis sets, and the ***A*** results were determined with DFT(PBE0) using fully balanced basis sets. [b]DFT (PBE and PBE0 functionals) was used at the optimized geometry for calculations of ***A***. [c]Calculation at the experimental geometry denoted by EXP and the one at the optimized geometry denoted by OPT. [d]Best calculated value calculated at the NEVPT2 level for ***g*** and ***D*** with the TZVP* basis set, and ***A*** with the fully balanced TZVP at PBE0 level, all at the optimized structure. [e]Ref 30. Experimental data. A significant difference is found with the original experimental assignment for 3-H′, 5-H′, 4-H, and 5-H. Therefore, we made a signal reassignment among these nuclei, with the result that the shifts are rendered into a very good agreement with the experiment.

It is found that dynamical correlation at the NEVPT2 level only has a minor effect on the results as compared to the CASSCF data. Such minor differences in the obtained shifts do not, *e.g.*, influence the relative order of the signals on the ppm scale. The differences found in the chemical shift values with NEVPT2 and CASSCF for nuclei 3-H, 4-H, 5-H, and B-H only amount up to 0.9, 0.1, 2.1, and 2.0 ppm, respectively.

The ***A***-tensor is a very sensitive parameter not only to the basis set, but it also varies greatly with the choice of the DFT functional. In this case we computed ***A*** with the PBE, PBE0, and PBE50 functionals. The comparison of results, with NEVPT2/TZVP* used for ***g*** and ***D***, is given in Table 4. It is found that there is a systematic and strong dependence of the shifts on the exact exchange admixture, as often seen in hyperfine properties. In its present usage, DFT is essentially an empirical method, with the exact exchange parameter that may be adjusted either to reproduce the possibly available *ab initio* results for ***A*** or the experimental chemical shifts. Using the latter criterion, presently the best agreement (see Figure S1 in the Supporting Information) with experiment is obtained with the 25% admixture of PBE0, for all shifts apart from that of 5-H. The relatively good performance of roughly this size of exact exchange incorporation (similar to the 20% of B3LYP) is often seen.[11]

The total chemical shifts for the experimental and optimized structures are compared in Table 4. There is a significant influence of the geometry optimization for the shifts of all but the 3-H nucleus. The resulting shifts are in good agreement with experimental values, with somewhat larger deviations found with the experimental X-ray structure as compared to the computationally optimized structure. The NMR experiments of ref 30 were carried out in the solution state. The positions of particularly the H atoms are not determined with good accuracy in X-ray experiments. Therefore, it is not surprising that the ^{1}H chemical shift results obtained with the geometry-optimized structure are superior to those with the X-ray geometry. Therefore, the choice of structure is important.

Our best estimates for the ^{1}H shifts are compared to experiment in Table 4. The computational result is based on NEVPT2/PBE0 calculations with TZVP*/QZVPP basis sets for ***g*** and ***D***/***A***, at the optimized geometry. A significant difference is found with the original experimental assignment for 3-H and 5-H. After a signal reassignment between these two nuclei, the results are brought to a qualitatively very good agreement with experiment. In fact, our best calculations are in a semiquantitative agreement for three of the four groups of protons. Only for 5-H we underestimate the (negative) shift by 21 ppm. The need to reassign can be due to different numbering conventions or a wrong experimental signal assignment.

3.3. System 2. Table 5 summarizes the calculated shifts for system 2, while all the calculated results are listed in Table S7 in the Supporting Information. The effect of the basis set used in calculating ***g*** and ***D*** is seen by comparing NEVPT2/PBE0 results obtained with SVP and TZVP basis. The data in Table 5 show that the difference of chemical shifts between SVP/SVP and TZVP*/SVP for nuclei 3-H, 4-H, 5-H, and B-H is 1.3, 0.1, 0.8, and 2.1 ppm, respectively, and practically identical changes are obtained between the sets SVP/TZVP and TZVP*/TZVP. Hence, similarly to system 1, there is only a very small effect of basis set for ***g*** and ***D***, whereas much larger effects of the basis set used in calculating ***A*** are seen in Table 5.

It is found that there is a somewhat larger effect of dynamical correlation at the NEVPT2 level than for the system 1. In the case of system 2, the ***g***- and ***D***-tensors depend on the choice of the wave function, i.e., whether CASSCF or NEVPT2 is used. The corresponding changes of chemical shifts are also given in Table 5. These amount, for nuclei 3-H, 4-H, 5-H, and B-H, to 3.2, 0.4, 2.3, and 5.3 ppm, respectively, which represents a non-negligible dynamical correlation effect.

DOI: 10.1021/acs.jctc.5b00193
J. Chem. Theory Comput. XXXX, XXX, XXX−XXX

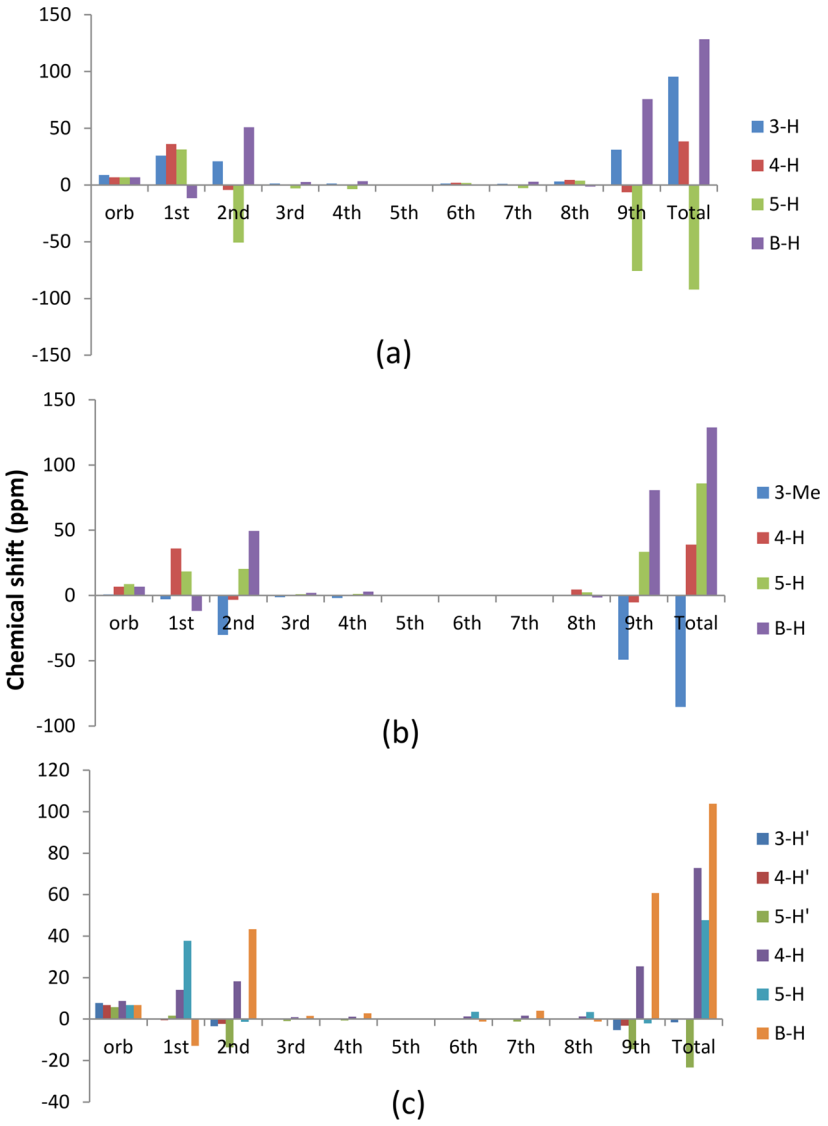

Figure 2. Physical contributions to the total calculated proton chemical shifts in (a) structure 1, (b) structure 2, and (c) structure 3. For the labeling of the nuclei, please refer to Figure 1, and for the numbering of the chemical shift contributions, see Table 1.

Similarly to system 1, ***A*** varies a great amount with the choice of DFT functional as seen in Figure S2 in the Supporting Information. This time, no unequivocal choice of functional can be made based on the experiment, however, as the functionals with different exact exchange admixtures fare best for the different protons. In particular, the 5-H signal, experimentally at 2.2 ppm, cannot be reproduced by any of the presently used functionals.

The total chemical shifts for experimental and optimized structures are compared with experiment in Table 5, for NEVPT2/PBE0 with TZVP*/TZVP basis sets. There is a large influence of using the optimized geometry instead of the X-ray geometry. For two nuclei, 4-H and B-H, the optimized structure leads to significantly improved shifts with respect to experiment. However, the agreement of the calculated 3-H shift with the measured value deteriorates at the same time. The best current chemical shift value calculated for the 5-H nucleus is 85.9 ppm, which is much larger than the experimental value of merely 2.2 ppm. In fact, all our calculations end up in such a big deviation for the 5-H signal. The reason for this behavior is unknown. It might be due to an experimental error in the signal assignment, such as due to a chemical impurity in the sample. On the computational side, intermolecular interactions, which we presently omit altogether, could contribute. On the basis of the present comparison of CASSCF and NEVPT2 data, it is likely that a more complete correlation treatment than what is feasible presently, would be helpful. However, the deviation from experiment for this single group of nuclei is most probably too large to be caused by an inadequate correlation treatment, either.

3.4. System 3. Largely similar findings apply to the largest present molecule, system 3, as what was seen for the two smaller systems. Table 6 gives a summary of the results, while Table S8 in the Supporting Information lists all the data.

System 3 features a somewhat larger dependence on the basis set used for ***g***, ***D***, and ***A*** than in the two smaller molecules. This finding may be connected to the fact that also the dynamical correlation effect, as measured from the difference between NEVPT2 and CASSCF results, is larger for system 3. As previously, the choice of the DFT functional does matter and PBE0 leads to an overall improved agreement with the (reassigned) experimental data, as compared to PBE. Similarly

DOI: 10.1021/acs.jctc.5b00193
J. Chem. Theory Comput. XXXX, XXX, XXX−XXX

to system 1 and 2, ***A*** varies with the choice of DFT functional as seen in Figure S3 in the Supporting Information. For this system, the chemical shifts are also very much dependent on the structure, i.e., whether it is X-ray-based or computationally optimized. In all cases but 4-H, the agreement with experiment is improved at the optimized structure, and even for this nucleus the observed deterioration is modest. The best computational results are mostly similar to the reassigned experimental data given in Table 6.

3.5. Physical Contributions to Proton Shifts. The different physical contributions to the total ^{1}H chemical shifts for systems 1−3 are illustrated in Figure 2. Besides the significant contact term (1st term) that varies in its sign and magnitude pattern across the aromatic protons and the BH proton, also the (2nd) dipolar term gives a large contribution. It is noteworthy that if ZFS interactions were neglected as in an earlier version of the formalism,[18] this dipolar term would give a strictly vanishing isotropic shift contribution. By far the most important term is, nevertheless, the pseudocontact term (term number 9). Both the terms 2 and 9 contain the same dipolar contribution to HFC and are seen to follow similar sign and magnitude patterns across the three systems. The corresponding tables of values for all the three systems are given in the Supporting Information.

4. CONCLUSIONS

We have applied modern pNMR chemical shift theory with the critical ***g***- and ZFS-tensors calculated using *ab initio* wave function theory, whereas DFT with different exchange-correlation functionals was used for the orbital shielding and hyperfine coupling tensors. The calculations were performed on the ^{1}H chemical shifts of three Co(II) pyrazolylborate complexes, for which experimental data were recently reported. The results obtained from these calculations are generally in good agreement with the experimental data, in some cases suggesting a reassignment of the experimental signals. The chemical shifts obtained with the *ab initio* CASSCF and NEVPT2 methods applied for the ***g***- and ZFS-tensors are more accurate than the all-DFT results. In the CASSCF/NEVPT2 calculations, locally dense basis sets are less expensive, yet accurate for ***g*** and ***D***. It is important to use a good basis for ***A***. Experimental X-ray and optimized structures lead to rather different results for the ^{1}H shifts. For one single ^{1}H shift in one of the compounds not even a qualitative agreement with the reported experimental datum could be found based on any of our calculations, and we suggest a new measurement to clarify the situation. The accuracy of the present mixed *ab initio*/DFT approach is very promising for further applications to demanding pNMR problems involving transition-metal systems.

■ ASSOCIATED CONTENT

Ⓢ Supporting Information

Optimized structures of the Co(II) complexes in the .xyz format; calculated DFT shieldings of the TMS reference molecule; tables of D and E/D values, as well as the g-factors obtained by DFT and CASSCF/NEVPT2 methods for system 1; tables of the calculated ^{1}H chemical shift values for systems 1−3; plots of chemical shifts with different functionals for systems 1−3; tables of the physical contributions to the total chemical shift for systems 1−3. This material is available free of charge via the Internet at http://pubs.acs.org.

■ AUTHOR INFORMATION

Corresponding Author

*Phone: 358 (0)40 1966658. Fax: 358 (0)8 5531287. E-mail: juha.vaara@iki.fi.

Notes

The authors declare no competing financial interest.

■ ACKNOWLEDGMENTS

The research leading to these results has received funding from the People Programme (Marie Curie Actions) of the European Union's Seventh Framework Programme FP7/2007-2013 under REA grant agreement no. 317127. Computational resources were partially provided by CSC-IT Center for Science (Espoo, Finland) and the Finnish Grid Initiative project. The work of J.M. and J.V. was supported by the directed programme in Computational Science of the Academy of Finland.

■ REFERENCES

(1) Levitt, M. H. *Spin Dynamics: Basics of Nuclear Magnetic Resonance*, 2nd ed.; Wiley; Chichester, 2007.
(2) Bertini, I., Luchinat, C., Parigi, G. *Solution NMR of Paramagnetic Molecules*; Elsevier; Amsterdam, 2001.
(3) Keizers, P. H. J.; Ubbink, M. *Prog. Nucl. Magn. Reson. Spectrosc.* **2011**, *58*, 88.
(4) Grey, C. P.; Dupré, N. *Chem. Rev.* **2004**, *104*, 4493.
(5) Kaupp, M.; Köhler, F. H. *Coord. Chem. Rev.* **2009**, *253*, 2376.
(6) Ramsey, N. F. *Phys. Rev.* **1950**, *78*, 699.
(7) Ramsey, N. F. *Phys. Rev.* **1952**, *86*, 243.
(8) Ramsey, N. F. *Phys. Rev.* **1953**, *91*, 303.
(9) Helgaker, T.; Jaszuński, M.; Ruud, K. *Chem. Rev.* **1999**, *99*, 293.
(10) *Calculation of NMR and EPR Parameters: Theory and Applications*; Kaupp, M., Bühl, M., Malkin, V. G., Eds.; Wiley-VCH: Weinheim, 2004.
(11) Vaara, J. *Phys. Chem. Chem. Phys.* **2007**, *9*, 5399.
(12) Autschbach, J. In *High Resolution NMR Spectroscopy*; Contreras, R. H., Ed.; Elsevier: Amsterdam, 2013; Vol. 3, p 69.
(13) Vaara, J. In *High Resolution NMR Spectroscopy*; Contreras, R. H., Ed.; Elsevier: Amsterdam, 2013; Vol. 3, p 41.
(14) McConnell, H. M.; Chesnut, D. B. *J. Chem. Phys.* **1958**, *28*, 107.
(15) McConnell, H. M.; Robertson, R. E. *J. Chem. Phys.* **1958**, *29*, 1361.
(16) Kurland, R. J.; McGarvey, B. R. *J. Magn. Reson.* **1970**, *2*, 286.
(17) Moon, S., Patchkovskii, S. In *Calculation of NMR and EPR Parameters: Theory and Applications*; Kaupp, M., Bühl, M., Malkin, V. G., Eds.; Wiley-VCH:Weinheim, 2004; p 325.
(18) Pennanen, T. O.; Vaara, J. *J. Chem. Phys.* **2005**, *123*, 174102.
(19) Pennanen, T. O.; Vaara, J. *Phys. Rev. Lett.* **2008**, *100*, 133002.
(20) Van den Heuvel, W.; Soncini, A. *Phys. Rev. Lett.* **2012**, *109*, 073001.
(21) Soncini, A.; Van den Heuvel, W. *J. Chem. Phys.* **2013**, *138*, 021103.
(22) Autschbach, J.; Patchkovskii, S.; Pritchard, B. *J. Chem. Theory Comput.* **2011**, *7*, 2175.
(23) Aquino, F.; Pritchard, B.; Autschbach, J. *J. Chem. Theory Comput.* **2012**, *8*, 598.
(24) Komorovsky, S.; Repisky, M.; Ruud, K.; Malkina, O. L.; Malkin, V. G. *J. Phys. Chem. A* **2013**, *117*, 14209.
(25) Van den Heuvel, W.; Soncini, A. *J. Chem. Phys.* **2013**, *138*, 054113.
(26) Martin, B.; Autschbach, J. *J. Chem. Phys.* **2015**, *142*, 054108.
(27) Schmitt, S.; Jost, P.; Van Wüllen, C. *J. Chem. Phys.* **2011**, *134*, 194113.
(28) Kubica, A.; Kowalewski, J.; Kruk, D.; Odelius, M. *J. Chem. Phys.* **2013**, *138*, 064304.
(29) Levine, N. I. *Quantum Chemistry*; Prentice Hall: NJ, 1991.

DOI: 10.1021/acs.jctc.5b00193
J. Chem. Theory Comput. XXXX, XXX, XXX−XXX

(30) Długopolska, K.; Ruman, T.; Danilczuk, M.; Pogocki, D. *Appl. Magn. Reson.* **2008**, *35*, 271.
(31) Roos, B. O. *Chem. Phys. Lett.* **1972**, *15*, 153.
(32) Angeli, C.; Cimiraglia, R.; Evangelisti, S.; Leininger, T.; Malrieu, J. P. *J. Chem. Phys.* **2001**, *114*, 10252.
(33) Angeli, C.; Cimiraglia, R.; Malrieu, J. P. *Chem. Phys. Lett.* **2001**, *350*, 297.
(34) Angeli, C.; Cimiraglia, R.; Malrieu, J. P. *J. Chem. Phys.* **2002**, *117*, 9138.
(35) Angeli, C.; Borini, S.; Cimiraglia, R. *Theor. Chem. Acc.* **2004**, *111*, 352.
(36) Neese, F. ORCA, *An ab Initio, Density Functional and Semiempirical Program Package*, Version 3.0.1, 2012.
(37) Perdew, J. P.; Burke, K.; Ernzerhof, M. *Phys. Rev. Lett.* **1996**, *77*, 3865; **1997**, *78*, 3865(E).
(38) Adamo, C.; Barone, V. *J. Chem. Phys.* **1999**, *110*, 6158.
(39) Rinkevicius, Z.; Vaara, J.; Telyatnyk, L.; Vahtras, O. *J. Chem. Phys.* **2003**, *118*, 2550.
(40) Arbuznikov, A. V.; Vaara, J.; Kaupp, M. *J. Chem. Phys.* **2004**, *120*, 2127.
(41) Liimatainen, H.; Pennanen, T. O.; Vaara, J. *Can. J. Chem.* **2009**, *87*, 954.
(42) TURBOMOLE V6.5 2013, a development of University of Karlsruhe and Forschungszentrum Karlsruhe GmbH, TURBOMOLE GmbH: 1989−2007, since 2007. Available from http://www.turbomole.com (accessed March 27, 2015).
(43) Lee, C.; Yang, W.; Parr, R. G. *Phys. Rev. B* **1988**, *37*, 785.
(44) Becke, A. D. *J. Chem. Phys.* **1993**, *98*, 5648.
(45) Stephens, P. J.; Devlin, F. J.; Ashvar, C. S.; Chabalowski, C. F.; Frisch, M. J. *J. Phys. Chem.* **1994**, *98*, 11623.
(46) Weigend, F.; Ahlrichs, R. *Phys. Chem. Chem. Phys.* **2005**, *7*, 3297.
(47) Weigend, F. *Phys. Chem. Chem. Phys.* **2006**, *8*, 1057.
(48) Dolg, M.; Wedig, U.; Stoll, H.; Preuss, H. *J. Chem. Phys.* **1987**, *86*, 866.
(49) Martin, J. M. L.; Sundermann, A. *J. Chem. Phys.* **2001**, *114*, 3408.
(50) Frisch, M. J.; Trucks, G. W.; Schlegel, H. B.; Scuseria, G. E.; Robb, M. A.; Cheeseman, J. R.; Scalmani, G.; Barone, V.; Mennucci, B.; Petersson, G. A.; Nakatsuji, H.; Caricato, M.; Li, X.; Hratchian, H. P.; Izmaylov, A. F.; Bloino, J.; Zheng, G.; Sonnenberg, J. L.; Hada, M.; Ehara, M.; Toyota, K.; Fukuda, R.; Hasegawa, J.; Ishida, M.; Nakajima, T.; Honda, Y.; Kitao, O.; Nakai, H.; Vreven, T.; Montgomery, J. A., Jr.; Peralta, J. E.; Ogliaro, F.; Bearpark, M.; Heyd, J. J.; Brothers, E.; Kudin, K. N.; Staroverov, V. N.; Kobayashi, R.; Normand, J.; Raghavachari, K.; Rendell, A.; Burant, J. C.; Iyengar, S. S.; Tomasi, J.; Cossi, M.; Rega, N.; Millam, J. M.; Klene, M.; Knox, J. E.; Cross, J. B.; Bakken, V.; Adamo, C.; Jaramillo, J.; Gomperts, R.; Stratmann, R. E.; Yazyev, O.; Austin, A. J.; Cammi, R.; Pomelli, C.; Ochterski, J. W.; Martin, R. L.; Morokuma, K.; Zakrzewski, V. G.; Voth, G. A.; Salvador, P.; Dannenberg, J. J.; Dapprich, S.; Daniels, A. D.; Farkas, O.; Foresman, J. B.; Ortiz, J. V.; Cioslowski, J.; Fox, D. J. GAUSSIAN 09, Revision D.01; Gaussian, Inc.; Wallingford, CT, 2009.
(51) Neese, F. *J. Chem. Phys.* **2003**, *118*, 3939.
(52) Neese, F. *J. Chem. Phys.* **2005**, *122*, 034107.
(53) Neese, F. *J. Chem. Phys.* **2007**, *127*, 164112.
(54) Chesnut, D. B.; Moore, J. *J. Comput. Chem.* **1989**, *10*, 648.
(55) Jensen, J. H.; Gordon, M. S. *J. Comput. Chem.* **1991**, *12*, 421.
(56) DiLabio, G. A.; Pratt, D. A.; LoFaro, A. D.; Wright, J. S. *J. Phys. Chem. A* **1999**, *103*, 1653.

DOI: 10.1021/acs.jctc.5b00193
J. Chem. Theory Comput. XXXX, XXX, XXX−XXX